Adipose transplantation improves olfactory function and neurogenesis via PKCα-involved lipid metabolism in Seipin Knockout mice

Jing Yang
Shanxi Medical University
Na Yang
Shanxi Medical University
Huifang Zhao
Shanxi Medical University
Yan Qiao
Chinese Academy of Sciences Institute of Coal Chemistry
Yanqiu Li
Chinese Academy of Sciences Institute of Coal Chemistry
Chunfang Wang
Shanxi Medical University
Kah-Leong Lim
Nanyang Technological University
Chengwu Zhang
Shanxi Medical University
Wulin Yang
Chinese Academy of Sciences Hefei Institutes of Physical Science
Li Lu (✉ luli@sxmu.edu.cn)
Shanxi Medical University https://orcid.org/0000-0003-2523-3372

Research Article

Keywords: Lipid metabolism, SVZ, Neurogenesis, Adipose transplantation, PKCα

Posted Date: August 24th, 2022

DOI: https://doi.org/10.21203/rs.3.rs-1948538/v1

Version of Record: A version of this preprint was published at Stem Cell Research & Therapy on September 7th, 2023. See the published version at https://doi.org/10.1186/s13287-023-03463-9.

Abstract

Lipodystrophy-associated Metabolic Disorders caused by Seipin deficiency lead to not only severe lipodystrophy but also neurological disorders. However, the underlying mechanism of Seipin deficiency-induced neuropathy is not well elucidated and the possible restorative strategy needs to be explored. In the present study, we investigated the systemic lipid metabolic abnormalities of Seipin knockout (KO) mice and their effect on adult neurogenesis in the subventricular zone (SVZ) and olfactory function. It was found that KO mice presented an ectopic accumulation of lipid in the lateral ventricle, accompanied by decreased neurogenesis in adult SVZ, diminished new neuron formation in the olfactory bulb, and impaired olfactory-related memory. Transcriptome analysis showed that the differentially expressed genes (DEGs) in SVZ tissues of adult KO mice were significantly enriched in biological processes related to lipid metabolism. Mass spectrometry imaging showed that the levels of glycerophospholipid, diglyceride and ceramide were significantly increased. In the restorative study, we found that subcutaneous adipose tissue transplantation (AT) rescued the abnormality of peripheral metabolism in KO mice and ameliorated the ectopic lipid accumulation in SVZ, concomitant with restoration of the SVZ neurogenesis and olfactory function. Mechanistically, PKCα was the potential mediator of lipid dysregulation-induced phenotypes. In the brain tissue of KO mice, PKCα was upregulated, which could be mimicked by the administration of DG analogue (Dic8) into cultured neural stem cells (NSCs). Dic8 impaired proliferation and differentiation NSCs, whereas it could be recovered by PKCα inhibitor. Overall, this study demonstrates that Seipin deficiency leads to systemic lipid metabolism disorder, which impairs neurogenesis and olfactory memory. Adipose transplantation restores lipid metabolic homeostasis and neurogenesis via PKCα involved pathway. The present study paves a novel way to treat lipid metabolic dysregulation-induced neurological disorders.

Introduction

Adipose tissue is an endocrine organ rather than an inert tissue that stores fat. Adipose tissue can synthesize many biologically active compounds that regulate metabolic homeostasis [5]. Seipin is the critical mediator of lipid biogenesis and metabolism [32], highly expressed in the adipose tissue and the brain [30]. BSCL2, the Seipin coding gene, deficiency is responsible for type 2 congenital generalized lipodystrophy (CGL2), a rare autosomal disorder. CGL2 is characterized by the absence of whole-body adipose tissue and metabolic disorders such as hepatic steatosis, insulin resistance (IR) and dyslipidemia [20]. Noteworthy, individuals with CGL2 have an increased prevalence of mild mental retardation, which is not usually observed in CGL1 [10, 38]. Given the abundant expression of Seipin in the brain, its role in the central nervous system remains to be explored. Animal models have also shown that impaired spatial memory and depression are also observed in mice with neuronal conditional knockout of Seipin, which may be related to impaired hippocampal neurogenesis [19].

In adult mammalian, neurogenesis exists in two main regions, the subgranular layer of the dentate gyrus in the hippocampus and the subventricular zone (SVZ) of the lateral ventricle. The blood-brain barrier (BBB) is more permeable in SVZ than in other brain regions [29]. Neural stem cells (NSCs) of SVZ extend

a minute apical ending to contact the ventricle and a long basal process ending on blood vessels, enabling them to exchange materials directly with the cerebrospinal fluid and bloodstream [14]. In addition, NSCs residing in SVZ continually generate new neurons that integrate into pre-existing circuits and participate in cognitive functions such as perceptual learning and olfactory memory [14, 23]. Impaired olfactory function is the essential prodromal symptom of neurodegenerative diseases such as Alzheimer's disease (AD) and Parkinson's Disease (PD) [11, 39].

Lipid biosynthesis and fatty acid metabolism genes are highly expressed in NSCs of SVZ [3, 33], indicating the involvement of lipid metabolism in NSCs biogenesis. Aberrant lipid metabolism is strongly implicated in neurological disorders [8, 18, 28]. Obese mice showed the accumulation of lipid droplets (LD) in SVZ, which impairs NSCs differentiation [28]. Additionally, lipid metabolic alteration is the causative factor for AD. Accumulation of oleic acid-rich triglycerides was found in the SVZ of patients with AD and 3xTg-AD mice, directly affecting NSCs activity. These results suggest that chronic diseases related to lipid metabolism disorders may lead to neurogenesis damage in SVZ, and there may be a common underlying mechanism among them [42].

In this study, we used KO mice with systemic lipid dysregulation as a model to investigate the association between lipid metabolism disorders and SVZ neurogenesis and olfactory dysfunction, and to explore potential common mechanisms and intervention strategies. It was found that olfactory-related memory significantly declined in adult KO mice compared to juvenile. Consistently, the proliferation and differentiation of NSCs were reduced considerably in adult KO mice. In addition, lipid ectopic accumulation in the SVZ region was observed in adult KO mice, including diacylglycerol (DG), phosphatidic acid (PA), phosphatidylcholine (PC), phosphatidylethanolamine (PE), and triglyceride (TG). Noteworthy, subcutaneous adipose tissue transplantation restored lipid metabolic homeostasis and neurobehavior dysregulation of KO mice. Mechanistically, PKCα overactivation got involved in Seipin deficiency-induced lipid metabolism and neurological dysregulation. We found that PKCα expression was upregulated in SVZ tissues of KO. Treatment of cultured NSCs with DG analogue Dic8 could also lead to upregulation of PKCα and damage the proliferation and differentiation of NSCs, while treatment with Go6983, an inhibitor of PKCα, could reverse this process. The present study elucidated the underlying mechanism of lipid metabolism disorders leading to neurobehavioral abnormalities. This may open a new way to treat neurological diseases caused by dysregulation of lipid metabolism.

Materials And Methods

Mice

C57/BL6 mice were obtained from the Animal Center of Shanxi Medical University and Seipin heterozygous mice (Seipin$^{+/-}$) were generously donated by Prof. Han Weiping (Agency for Science, Technology and Research, Singapore). All animal studies were performed in accordance with the Institutional guidelines approved by the Animal Research Ethics Committee of Shanxi Medical University. Seipin$^{+/-}$ mice were bred and inter-crossed to obtain homozygous knockout (Seipin knockout, KO) mice

along with C57/BL6 wild type (WT) mice. All mice were kept in an animal facility maintained at 22℃ ± 2℃ under a 12 h light/dark cycle. Food and water were available ad libitum.

NSCs culture and DG treatment

Primary NSCs cultures were prepared from the SVZ of neonatal mice following the protocol established previously [46]. Briefly, Cells were plated at 1 × 10^5 cells/mL and cultured in DMEM-F12 proliferation medium supplemented with 2% B27 (Invitrogen, Stockholm, Sweden), 20 ng/mL epidermal growth factor (EGF; PeroTech, Rocky Hill, NJ, USA), and 20 ng/mL basic fibroblast growth factor (bFGF; PeroTech) in a humidified incubator at 37 °C with 5% CO2. After a week of culture, neurospheres were gained and digested with Accutase Cell Detachment Solution (Gibco) to obtain single cell suspension. Then NSCs were plated onto the coverslips pre-coated with 50 μg/ mL poly-L-ornithine and 20 μg/mL laminin (Sigma-Aldrich, Saint Louis, MO, USA) overnight. To measure the effect of DG on NSCs proliferation, cells were treated with 50 μM and 100 μM DiC8 (Aladdin Chemistry Co, Shanghai, China) or PKC inhibitor (Go6983; 140 nM; MedChemExpress, Monmouth Junction, NJ, USA) and cultured in DMEM supplemented with BrdU (10 μM) for 12 h for immunofluorescence analysis. For NSCs differentiation, the culture medium was replaced with differentiation medium containing 1% fetal bovine serum, 1% B27 supplement, DiC8, and/or Go6983. After three days, cells were harvested for immunostaining.

Brain dissection and tissue processing

Mice fixed by transcardiac perfusion with 4% paraformaldehyde (PFA) after anaesthetization. Brains were carefully dissected and post-fixed overnight. After dehydration in 30% sucrose, OCT (Sakure, Tokyo, Japan) embedded brains were sliced into serial free-floating sections cut at 16 μm thickness using a cryostat (Leica Microsystems, Wetzlar, Germany). One of every six consecutive sections encompassing the SVZ (bregma 1.09 mm to 0.13mm) or the olfactory bulb (bregma 4.57mm to 4.07mm) was selected for immunostaining.

Immunofluorescence staining

For immunofluorescent staining, 4% PFA-fixed sections or cells were permeabilized with 0.3% Triton X-100 (Sigma-Aldrich) in PBS for 15-20 min and blocked with 10% goat serum for 1 h at room temperature (RT). The specimens were incubated with primary antibodies overnight at 4℃. The primary antibodies used in the present study are listed in Table 1. Goat anti-rabbit IgG H & L (Alexa Fluor 555), Goat anti-mouse IgG H & L (Alexa Fluor 555), and Goat anti-mouse IgG H & L (Alexa Fluor 488) were used as appropriate secondary antibodies and incubated for 1 h at RT. Nuclei were counterstained with 4,6-diamidino-2-phenylinedole, dihydrochloride (DAPI; Sigma-Aldrich) at 1 mg/ml for 5 min.

Sections for BrdU staining were denatured to expose antigen with 2 M HCl at 37°C for 10-15 min in tissues before the Triton X-100 treatment. The sections are then incubated successively with anti-BrdU antibody overnight at 4°C. Then, Alexa Fluor 488 goat anti-mouse IgG for 1 h at RT. The fluorescence images were captured by Olympus BX51 microscope (Olympus, Tokyo, Japan) or Leica SP8 confocal microscope (Leica Microsystems).

Quantitation of fluorescent images

The fluorescent images were analyzed in a double-blinded manner using MetaMorph software (Molecular Devices, Sunnyvale, CA, USA) from at least three independent experiments. Serial sections from comparable positions were used to count positive cells in vivo, as reported previously [27]. For each mouse, 6 sections were counted and the average number of $Ki67^+$ and DCX^+ cells in each area was calculated, then multiplied by the number of sections per SVZ to obtain the total number per mouse. For the olfactory bulb, 6 sections were taken and the average number of $BrdU^+/NeuN^+$ cells was calculated. In vitro, for each coverslip, six different non-overlapping regions were randomly selected at 20-fold magnification and the percentage of $BrdU^+$ and $Tuj1^+$ cells were calculated.

Olfactory habituation/dishabituation test

To assess the olfactory bulb function, olfactory habituation/dishabituation tests were performed. Before the test, each mouse was placed in the chamber (31 × 25 × 12.5 cm) for 30min to acclimate new environment. For each test, the odors were detected in the following order: mineral oil, isoamyl acetate (IAA), vanilla (1 mg/ml), female mice urine and male mice urine, and the testes were repeated three times, at 1 min intervals. Successive trials with different odors were separated by 5 min. The duration of sniffing behavior toward each odor stimulus was recorded.

Olfactory short-term memory text

The olfactory short-term memory test was conducted to assess the ability of mice to recognize familiar odors. Mice habituated to experimental conditions during the adaptation phase were placed in a 31 × 25 × 12.5 cm chamber. Mice were subjected to odorants dropped on filter paper (2 × 2 cm) for 5 min at 30, 60, 90, or 120 min intervals. A different odor was used at each interval point, but each mouse was tested at only one interval per day to avoid cross interference of olfactory detection and memory. If mice remembered the odor from the 1st trial, they were expected to spend less time sniffing when subjected to odorant for the 2nd time.

Olfactory avoidance test

Olfactory avoidance behavior to nondehydrogenated 2, 4, 5-trimethylthiazole (nTMT), a synthetic fox feces odor, was recorded to assess mice olfactory sensitivity. During the adaptation phase, each mouse was acclimated in a cage of the same size as the test cage (31 × 25 × 12.5 cm) for 30 min, then transferred to a new test cage for 30 min, and repeated four times. During the test phase, the test cage was divided into two equal areas, then nTMT was added to the filter paper (2 × 2 cm) on one side of the test cage at the concentration of 0%, 16%, and 12%, respectively. The mice were placed in the middle of the test cage, and the time they stayed on the other side of the cage was observed and recorded for 10 min.

Oil Red O staining

The frozen SVZ sections mounted on superfrost glass slides were allowed to air dry for 12 h at RT. After air drying, the slides were placed in 60% isopropanol for 1-3s and stained with Oil Red O solution (Sigma-Aldrich) for 10 min. Next, the sections were washed with distilled water, rinsed with 60% isopropanol for 1 min, and washed for another 5 min. The staining of slides was imaged using a microscope (Olympus). The area and intensity of LD in the SVZ ventricle wall were quantified by Adobe Photoshop software, and normalized by the lateral ventricle perimeter in each image. The intensity was quantified in three different subregions of SVZ, a depth of 20 μm from the ventricular wall.

Adipose transplantation (AT)

AT was performed on mice at one-month-old and littermates were used to avoid rejection. Subcutaneous adipose tissue of euthanized donor mice was taken and cut into 1 cubic centimeter pieces. Recipient mice were anesthetized with 2.5% isoflurane (Abbott, Baar, Switzerland) and a small incision (1 cm^3) was created in the back. The graft (500 - 900mg) was inserted through a syringe into the subcutaneous space through the incision. Sham-operated control mice received the same operation but without adipose injection. After surgery, incisions were closed using 4-0 silk sutures. When the mice were fully awake, they were sent back to the animal room for feeding and observation. AT was performed once a month and continued for 4 months. During this period, the liver/body weight was recorded. Before sacrifice, the adipose tissue was evaluated visually by IRIS PET/CT (Inviscan SAS, Strasbourg, France). The HU value of the adipose tissue was between -300 and -100. After the identification of adipose tissue, the region-growing thresholding algorithm was used to estimate adipose tissue volume with a very bright adipose signal by OsiriX imaging software (OsiriX Foundation, Geneva, Switzerland)). Adipose weight was calculated by multiplying the adipose volume and the adipose density. For histological evaluation of transplanted tissue, adipose tissue was removed 4 months after transplantation. Following formalin fixation, adipose tissues were paraffin-embedded, and 4 μm paraffin sections were stained with hematoxylin and eosin (HE).

HE staining

The fresh dissected adipose tissue was fixed with a fixator for more than 24 h and subjected to alcohol gradient dehydration. Then, the wax-soaked adipose tissue was embedded and placed in the paraffin slicer for sectioning to a 4 μm slice. The paraffin sections were dewaxed and dyed with hematoxylin solution (Servicebio, Wuhan, China) for 3 - 5 min. Hematoxylin Differentiation solution (Servicebio) was differentiated for 2 - 5 s, and the Hematoxylin Scott Tap Bluing (Servicebio) was treated for 2 – 5 s. The slices were dyed in eosin solution (Servicebio) for 5 min and then placed in gradient alcohol and xylene for 5min respectively, and sealed with neutral gum. Lastly, the tissue sections were observed under the Olympus BX51 microscope (Olympus) and the images were collected for analysis.

Calculation of liver to Body weight ratio

Body weight and wet liver weight were recorded immediately after the experimental animals were sacrificed. The liver to body weight ratio was calculated using the formula: liver weight (g) x 100 / body weight (g).

Determination of plasma adiponectin and leptin levels

Serum was collected after 1000 rpm centrifugation. Adiponectin and leptin levels were measured using a specific ELISA kit (Cloud-Clone Corp, Wuhan, China). Sample dilution and standard calibrators were prepared following kit instructions. Briefly, ELISA plate coated with capture antibody were incubated with 100 μL test samples or standard at 37℃ for 2 h, and then biotinylated antibody was added and incubated at 37℃ for 1 h. After washing away the unbound biotinylated antibody, the HRP labeled avidin was added. Tetramethylbenzidine substrate was added following an additional washing step. The absorbance (OD value) was measured at 450 nm wavelength excitation using a microplate reader (BioTek Instruments, Winooski, VT, USA) to calculate the sample concentration.

Glucose and insulin tolerance tests

For glucose tolerance assay, mice were intraperitoneally injected with 2mg/kg of glucose after 6 h fasting. Blood samples were collected from the tail vein. Glucose values were measured at 0, 15, 30, 60, 90, and 120 min post-injection with a glucometer (Johnson & Johnson, New Brunswick, NJ, USA). For insulin tolerance assay, mice were injected intraperitoneally with 0.75 mIU/g insulin after 4 h fasting, and glucose levels were measured at 0, 15, 30, 60, and 90 min post-injection.

Matrix-assisted laser desorption ionization time-of-flight mass spectrometry (MALDI-TOF MS) analysis

The SVZs of mice were dissected on ice and placed in the tissue-homogenizing tube, which was frozen in liquid nitrogen. The frozen tissue block was sliced into 12 μm thickness sections by cryostat microtome (Leica Microsystems) and thaw-mounted onto indium tin oxide (ITO)-coated glass slides. After the above slices into ITO were dried, they were sprayed with O–P, N-C/G solution as the matrix (1 mg/mL) by using an automated spraying device (HTX Technologies LLC, Carrboro, NC, USA) and dried thoroughly in a vacuum desiccator[45]. Then, the SVZs tissues were identified by MALDI-TOF MS and all analyses were performed with an UltrafleXtreme mass spectrometer (Bruker Daltonics, Bremen, Germany). The imaging software conducted the MALDI-TOF MS data from three different subregions of the lateral ventricles at a depth of 20 μm surrounding the ventricular wall. Two-dimensional ion density maps for different compound mass-to-charge ratios (m/z) were obtained after smoothing and baseline calibration with SCiLS Lab 2020a software. Significantly different m/z values ($p < 0.05$) between the two groups were obtained based on ROC analysis and t-tests in SCiLS Lab 2020a software.

RNA isolation and transcriptome analysis

The total RNA of SVZ was isolated by TRIzol reagent (Molecular Research Center, Cincinnati, Ohio, USA) according to the manufacturer's instructions. Transcriptome sequencing and data analysis were completed by Biomarker Technologies Company (Beijing, China). Hierarchical cluster analysis based on the differentially expressed genes (DEGs) was filtered with *p*-value < 0.05, and log2 fold change (Log2 FC) > 0.5 or < −0.5 in each pairwise comparison. The Gene Ontology (GO) enrichment and the Kyoto Encyclopedia of Genes and Genomes (KEGG) were analyzed with KOBAS software.

Western Blotting

Cells or brain tissues were washed with ice-cold PBS and lysed in RIPA lysis buffer supplemented with the protease inhibitor cocktail (Thermo Fischer Scientific, Pittsburgh, PA, USA). Total protein concentration was determined using the BCA Protein Assay Kit (Beyotime Biotechnology). An equal amount of proteins were separated by 10% SDS-polyacrylamide gels and transferred to polyvinylidene difluoride membranes (Millipore, Billerica, MA, USA). The membrane was blocked in 5% milk in TBST (TBS containing 0.1% Tween-20) for 1 h at RT and incubated with primary antibodies overnight at 4℃. After washing in TBST, the membrane was incubated with horseradish-coupled secondary antibody for 2 h at RT. Immunoreactive protein bands were visualized using an ECL detection kit (Thermal Biotech, Rockford, IL, USA). The band intensities were quantified using Image-J software and densitometry values were normalized to the corresponding β-actin values. Antibodies utilized here are listed in Table 1.

Statistical Analysis

All experiments were repeated at least three times. All statistical analyses were performed using Prism software (GraphPad Software, San Diego, CA) and presented as mean standard deviations (SD). The

unpaired Student's t-test was used for comparisons between two groups, and two-Way ANOVA with Tukey's post-hoc test was used for multi-group comparisons. The *p*-value < 0.05 was selected to determine statistical significance.

Results

Impaired olfactory function and SVZ neurogenesis in adult KO mice

Since olfactory dysfunction is an early symptom of neurodegenerative diseases [11, 25], we firstly examined the olfactory function in Seipin deficiency mice. The odor habituation/dishabituation test showed that either juvenile (1-month-old) or adult (5-month-old) KO mice could sense odorants (**Fig. 1A**). For the short-term olfactory memory measurement, mice were presented with the same odorant twice with an interval between the two presentations. Generally, mice showed less interest in odorants that they had encountered previously. Compared with the first presentation, the sniffing duration of the second exposure was significantly decreased at four intervals (30, 60, 90, and 120 min) in Juvenile KO mice. However, adult KO mice exhibited a similar interest at the 60 min, 90 min and 120 min intervals, indicating that olfactory-related memory capacity was impaired in the adult stage (**Fig. 1B**). Considering adult SVZ neurogenesis is necessary for olfactory memory, NSCs proliferation and differentiation were measured by Ki67 and DCX staining. As displayed in **Fig. 2A and B**, the number of $Ki67^+$ cells and DCX^+ neurons in SVZ of adult KO mice was significantly decreased, rather than that of juvenile KO mice. Likely, the number of $BrdU^+/NeuN^+$ cells in the olfactory bulb of adult KO mice was considerably lower than that of control, further confirming the impairment of SVZ neurogenesis in adult KO mice (**Fig. 2C**). In vitro study showed that compared with WT control, the number of $BrdU^+$ proliferating cells and $Tuj1^+$ neurons in cultured NSCs from both neonatal and adult KO mice did not show significant alternation (**Fig. 2D and E**), indicating it might not be directly affected by Seipin deficiency. The above results indicated that in vivo SVZ neurogenesis and olfactory-related memory were significantly compromised in adult KO mice, which may be related to the altered tissue microenvironment of adult KO mice rather than the intrinsic loss of Seipin in NSCs.

Dysregulated lipid metabolism in SVZ region of adult KO mice

To investigate the possible mechanism underlying neurogenic disorders in adult KO mice, a high-throughput transcriptome analysis on SVZ tissues of KO mice was performed. As shown in **Fig. 3A and B**, DEGs were significantly enriched in metabolism-related biological processes in adult KO mice compared with juvenile KO mice, especially in lipid-related ones. Further analysis revealed that significant alterations concentrated in glycerophospholipid metabolism, phosphatidylinositol and sphingolipid metabolism signaling pathways (**Fig. 3C**). To identify potential molecules associated with lipid

metabolism disorders in the SVZ region of adult KO mice, MALDI-TOF MS was performed. It was shown that the contents of DG, PA, PC, PE, and TG increased significantly (**Fig. 3D-F**). Oil red staining showed a significant accumulation of LD in SVZ of adult KO mice (**Fig. 3G**). Pearson's correlation analysis demonstrated a significant negative correlation between LD accumulation area and neurogenesis in mice (**Fig. 3H**). These results indicated an abnormal lipid metabolism in the SVZ region of adult KO mice, which may cause impaired SVZ neurogenesis.

AT restored systemic metabolic homeostasis in KO mice

Seipin is the critical mediator of lipid metabolism and loss function of mutation of Seipin leads to a severe adipose deficit. AT holds the potential to restore a metabolic deficiency in KO mice. Adipose tissue was implanted under the dorsal skin of juvenile WT (WT-AT) mice and KO (KO-AT) mice, respectively, with sham-operation groups (WT-Sham, KO-Sham) as control. Four months later, whole-body CT scans were performed on four groups of adult mice. Coronal scan results showed severe loss of adipose tissue and fatty liver in the whole body of KO-Sham mice. In contrast, the dorsal adipose tissue distribution of KO-AT mice was comparable with that of WT-Sham mice (**Fig. 4A**), which was brightly colored, soft and mobile, and significantly vascularized (**Fig. 4B**). CT scan analysis of adipose volume showed that the surviving fat in KO-AT mice reached 365mg ± 84mg after transplantation (**Fig. 4C**). As shown in **Fig. 4D**, the morphology of transplanted adipocytes of KO-AT mice was similar to that of WT mice (**Fig. 4D**). Plasma levels of adiponectin and leptin were significantly increased in KO-AT mice compared with control mice. However, the levels of adiponectin and leptin were decreased in KO mice, indicating that the transplanted adipose tissue could perform normal endocrine functions (**Fig. 4E and F**). The ratio of liver weight to body weight in the KO-AT group was also markedly decreased. (**Fig. 4G**). Additionally, reduced blood glucose levels, enhanced glucose tolerance and improved insulin sensitivity were observed in KO mice after adipose transplantation (**Fig. 4H-J**). These data suggested that AT could effectively correct systemic metabolic disorders in KO mice.

AT rescued olfactory-related neurobehavior in KO mice

To determine whether AT improves neurological deficits in KO mice, immunofluorescence staining and behavioral experiments were performed. Although the number of $Ki67^+$ and DCX^+ in SVZ of KO-Sham group was significantly reduced compared with that of WT-Sham group, $Ki67^+$ proliferating cells and DCX^+ neurons in KO-AT group were considerably recovered (**Fig. 5A and B**). Further, $BrdU^+/NeuN^+$ double staining was applied to determine the number of neonatal neurons in the olfactory bulb granular layer. As shown in **Fig. 5C**, the number of $BrdU^+/NeuN^+$ neurons in the KO-AT mice was also significantly increased after AT (**Fig. 5C**). Behavioral tests did not demonstrate a significant difference in olfactory discrimination ability among all groups (**Fig. 5D**). However, olfactory short-term memory tests showed that the sniffing duration was significantly reduced in the KO-AT group compared to the KO-Sham group, indicating that AT could partially restore olfactory-related memory (**Fig. 5E**). Additionally, an odor avoidance test

was adopted to test the olfactory sensitivity. It was shown that when mice were given a solvent (0% nTMT), there was no significant difference of the residence time in the avoidance area. When subject to 6% nTMT, KO-AT mice demonstrated excellent odor avoidance compared to KO-Sham control. There was no difference between the two groups when nTMT concentrations reached 12%, which dulled the sense of smell (**Fig. 5F**). These results suggest that AT is beneficial to restore olfactory neurogenesis and olfactory memory in KO mice to a certain extent.

AT reduced the accumulation of diglycerides to alleviate the over-activation of PKCα

To elucidate the possible mechanism of neurobehavioral restoration in KO-AT mice, multiple assays were carried out. Oil red staining revealed that AT reduced abnormal lipid accumulation in SVZ in adult KO mice (**Fig. 6A**). MALDI-TOF MS results showed that AT decreased glycerophospholipid, TG and DG content in the SVZ of KO mice (**Fig. 6B and C**), indicating that AT is beneficial to the recovery of lipid homeostasis in SVZ region. Protein kinase C (PKC) family member, PKCα, was proved to involve in lipid metabolism[40]. Our gene differential analysis showed that PKCα was upregulated in SVZ tissues of adult KO mice (**Fig. S1**). Western blotting results confirmed that the level of PKCα in SVZ tissues of adult KO mice was increased, which was recovered by AT (**Fig. 6D**), implying that PKCα may mediate signal transduction and neurogenesis injury caused by lipid metabolism disorder in the SVZ region.

Notably, DG was not only the critical intermediate of phospholipids but also served as the second messenger to activate phospholipids and calcium-dependent enzyme PKC and regulate various biological procedures [4, 26, 40, 49]. The above experiments have found that DG was one of the most prominently altered molecules, which might be responsible for the activation of PKCα signaling. To further substantiate the idea, we applied DG analogue Dic8 to treat cultured NSCs. It showed that 12 h of Dic8 treatment significantly increased PKCα level in NSCs (**Fig. 6E**). BrdU and Tuj1 staining showed that the proliferation and differentiation ability of NSCs were significantly decreased after Dic8 treatment for 12 h, which could be rescued by PKCα inhibitor (**Fig. 6F and G**). These results suggested that the excessive lipid accumulation might exert its deleterious effect via activation of PKCα, which a PKCα inhibitor could ameliorate.

Discussion

Seipin is known as the critical regulator of lipid metabolism. Loss of function mutation of Seipin led to not only lipid dysregulation but also neurological deficits, and the latter attracted augmenting attention [7, 20]. In this study, we found abnormal lipid accumulation in SVZ of KO mice, accompanied by elevated glycerophospholipid and DG contents, resulting in abnormal SVZ neurogenesis, as well as olfactory memory dysfunction. Importantly, AT effectively relieved metabolic disorders in the SVZ region of KO mice, concomitant with restored SVZ neurogenesis and olfactory memory. Lipid metabolism mediator, PKCα, might get involved in KO-induced phenotypes since PKCα inhibitors restored the proliferation and

differentiation of NSCs compromised by DG analog in vitro. Optimistically, modulating systemic metabolism by AT or PKCα inhibition may serve as a practical approach to relieving lipid metabolic disorders and its induced intellectual disability (Fig. 7).

Seipin was abundantly expressed in the central nervous system, and Seipin deficiency mice exhibited impaired spatial memory and anxious-depression-like phenotype [47, 48]. Some studies reported that KO suppressed proliferation and differentiation of hippocampal NSCs, which was responsible for depression-like behavior [48]. But some studies demonstrated that Seipin deficiency did not alter the number of hippocampal neuronal cells [9, 31]. In the present study, we found that Seipin deficiency did not affect SVZ NSCs activity in vitro but significantly inhibited the proliferation and differentiation potential of SVZ NSCs in adult KO mice. This could attribute to the location of SVZ NSCs that were more susceptible to changes in the endocrine environment which was mediated by Seipin deficiency. For example, in the diabetes mice induced by intraperitoneal injection of streptozotocin, the proliferation and differentiation of NSCs in the SVZ region were suppressed concurrently with the down-regulation of insulin receptor β and glycogen synthase kinase 3β [17]. This inhibition was attenuated by adrenal corticosterone removal [12], indicating that SVZ NSCs could rapidly receive and respond to peripheral metabolic signals [44]. Our results also showed severe metabolic abnormalities in adult KO mice, accompanied by aberrant expression of metabolism-related genes in SVZ. It was reported that in SVZ of diabetes mice excessive adipose deposition was observed and neurogenesis was impaired accompanied by elevated inflammatory cytokines in the bloodstream [1, 28]. These studies supported the notion that the fate of NSCs in SVZ was susceptible to microenvironment variation.

The brain is a lipid-rich organ, and the distribution of lipids varies in different brain regions. MALDI-MSI analysis of the SVZ lipid composition in the human brain revealed that the SVZ was rich in sphingomyelin and phosphatidylserine (PS) but deficient in PE or PC [16]. The levels of glycerophospholipid in the brain with metabolic diseases such as obesity and diabetes also changed significantly, and the changes in the content of PC and DG were directly proportional to the severity of the disease [18, 34]. In the present study, we found that glycerophospholipids such as DG, PA, PE, and PC in the SVZ of KO mice were significantly increased. The transcriptome analysis results indicated that glycerophospholipid signaling pathway was abnormal in KO mice. AT transplantation rescued the disorder of SVZ lipid metabolism, significantly reducing the content of PS, PE and DG, as well as neurogenesis in KO mice.

Of the lipid metabolite, DG was an intermediate molecule of glycerophospholipid metabolism and participated in various biological processes. One of the important aspects was that aberrant elevation DG in the brain was closely related to neurological dysfunction. In AD and Sjogren-Larsson syndrome patients, elevated DG was reported to be accompanied by cognitive or intellectual impairment [34, 35, 43]. Another study reported that fatty acid metabolism in the SVZ region was disturbed in AD mouse model and patients as manifested by abnormal accumulation of oleic acid. Inhibition of the rate-limiting enzyme of oleic acid synthesis could rescue the defect of SVZ NSCs proliferation [35]. In the present study, we observed increased DG levels in the SVZ region of KO mice. In vitro, DG analog, Dic8,

suppressed the proliferation of NSCs, indicating the excessive accumulation of DG might account for impaired NSCs activity. These studies highlight that metabolic abnormality could directly affect NSCs activity, and maintaining metabolic balance may be an alternative strategy for treating metabolism-related neurological diseases.

PKCα belonged to the PKC family, which was involved in various cellular processes, including proliferation, differentiation, migration and metabolism [40]. The activity of PKC was closely correlated with lipid metabolism, possessing at least one C1 domain with a higher affinity for DG [40]. It was reported that activation of PKC by DG analogue induced the apoptosis of cerebellar granular cells and inhibited the differentiation of neural precursor cells, while PKC isoenzyme inhibitors attenuated the effects of DG accumulation [15, 36]. Another study reported that the increase of PKCα and its phosphorylation substrates in the AD brain leads to impaired neuronal function [2, 37]. PKCα inhibitors can block the endocytosis and synaptic inhibition of glutamate receptors produced by Aβ [2]. All those shreds of evidence suggested that PKCα participated in the lipid metabolites, especially DG, involved in neurological disorders. Here, we found that the expression of PKCα was increased in KO mice SVZ. In vitro, the addition of DG analog suppressed proliferation and differentiation of NSCs. Go6983, an inhibitor of PKCα, reversed the inhibitory effect of Dic8 on NSCs. Therefore, we presumed that the impaired SVZ neurogenesis in adult KO mice was partially caused by the activation of PKCα.

Adipose tissue not only served as an organ for energy storage, but also as an endocrine organ to regulate metabolic homeostasis of the body [21, 24]. AT has been widely used in plastic surgery and burn treatment due to its reproducibility, easy to obtain in large quantities and less damage to the donor [6, 13]. It was reported that transplantation of subcutaneous adipose tissue from normal mice into the subcutaneous region of KO mice restored peripheral metabolic balance and improved hepatic steatosis and kidney function [22, 41]. In the current work, AT fixed SVZ neurogenesis and olfactory function of KO mice accompanied by stabilized peripheral metabolism. Therefore, adipose transplantation presented a potential therapeutic strategy for congenital generalized lipodystrophy and its associated neurological deficiency. Collectively, the present study demonstrated that Seipin deficiency impaired the neurobehavioral function via dysregulating lipid metabolism, which could be rescued by AT. PKCα played a crucial role in this paradigm. AT and PKCα inhibition could serve as one strategy for the treatment of lipid dysregulation-involved diseases.

Abbreviations

AD
Alzheimer's disease
AT
adipose tissue transplantation
BBB
blood-brain barrier
bFGF

basic fibroblast growth factor
CGL2
type 2 congenital generalized lipodystrophy
DEGs
differentially expressed genes
DG
diacylglycerol
EGF
epidermal growth factor
GO
Gene Ontology
HE
hematoxylin and eosin
IAA
isoamyl acetate
IR
insulin resistance
ITO
indium tin oxide
KO
Seipin knockout
KEGG
Kyoto Encyclopedia of Genes and Genomes
LD
lipid droplets
LV
lateral ventricle
MALDI-TOF MS
Matrix-assisted laser desorption ionization time-of-flight mass spectrometry
NSCs
neural stem cells
nTMT
nondehydrogenated 2, 4, 5-trimethylthiazole
OB
olfactory bulb
PA
phosphatidic acid
PC
phosphatidylcholine
PD

Parkinson’s Disease
PE
phosphatidylethanolamine
PFA
paraformaldehyde
PKC
protein kinase C
PS
phosphatidylserine
RMS
rostral migratory stream
RT
room temperature
SD
standard deviations
SVZ
subventricular zone
TG
triglyceride
WT
wild type.

Declarations

Availability of data and materials

The datasets used and/or analyzed during the present study are available from the corresponding author on reasonable request.

Acknowledgements

This work was supported by grants to Li Lu, Chengwu Zhang and Jing Yang from the Natural Science Foundation of Shanxi Province (#20210302123291, #20210302123299 and #20210302124561), and the Research Project supported by Shanxi Scholarship Council of China (#2020-085), and to Kah-Leong Lim from the Science and Technology Cooperation and Exchange Project of Shanxi Province (#202104041101026). We thank Dr. Xiaowen Bai for helpful discussions.

Author information

Authors and Affiliations

Department of Anatomy, Shanxi Medical University, Taiyuan, People's Republic of China

Jing Yang, Na Yang, Li Lu

School of Basic Medical Sciences, Shanxi Medical University, Taiyuan, People's Republic of China

Chengwu Zhang, Huifang Zhao

Analytical Instrumentation Center & State Key Laboratory of Coal Conversion, Institute of Coal Chemistry, Chinese Academy of Sciences, Taiyuan, People's Republic of China

Yan Qiao, Yanqiu Li

Laboratory Animal Research Center of Shanxi Medical University, Shanxi Key Laboratory of Animal and Animal Model of Human Diseases, Shanxi Medical University, Taiyuan, People's Republic of China

Chunfang Wang

Lee Kong Chian School of Medicine, Nanyang Technological University, Singapore

Kah-Leong Lim

Anhui Province Key Laboratory of Medical Physics and Technology, Center of Medical Physics and Technology, Hefei Institutes of Physical Science, Chinese Academy of Sciences, Hefei, People's Republic of China

Wulin Yang

Cancer Hospital, Hefei Institutes of Physical Science, Chinese Academy of Sciences, Hefei, People's Republic of China

Wulin Yang

Key Laboratory of Cellular Physiology, Ministry of Education, Shanxi Medical University, Taiyuan, People's Republic of China

Li Lu

Contributions

Jing Yang and Na Yang conducted the experiments, analyzed the data, and prepared the figures. Na Yang, Huifang Zhao, Yanqiu Li and Yan Qiao helped in some MALDI-TOF MS experiments. Chunfang Wang helped in some animal experiments. Chengwu Zhang, Wulin Yang, Kah-Leong Lim and Li Lu conceived and designed the research. The manuscript was written by Jing Yang, Li Lu, Wulin Yang and Chengwu Zhang.

All authors read and approved the final manuscript.

Author notes

Jing Yang and Na Yang are co-first authors.

Corresponding authors

Correspondence to Chengwu Zhang, Wulin Yang, or Li Lu.

Ethics declarations

All animal studies were approved by the Committee for Animal Care and Ethical Review at Shanxi Medical University.

Consent to participate

Not applicable.

Consent for publication

Not applicable.

Competing interests

The authors declare that they have no competing interests.

References

1. Acosta JC, Banito A, Wuestefeld T, Georgilis A, Janich P, Morton JP, Athineos D, Kang TW, Lasitschka F, Andrulis Met al. A complex secretory program orchestrated by the inflammasome controls paracrine senescence. Nat Cell Biol. 2013;15:978–90. Doi 10.1038/ncb2784.
2. Alfonso SI, Callender JA, Hooli B, Antal CE, Mullin K, Sherman MA, Lesne SE, Leitges M, Newton AC, Tanzi REet al (2016) Gain-of-function mutations in protein kinase Calpha (PKCalpha) may promote synaptic defects in Alzheimer's disease. Sci Signal 9: ra47 Doi 10.1126/scisignal.aaf6209.
3. Borrett MJ, Innes BT, Tahmasian N, Bader GD, Kaplan DR, Miller FD. (2022) A Shared Transcriptional Identity for Forebrain and Dentate Gyrus Neural Stem Cells from Embryogenesis to Adulthood. eNeuro 9: Doi 10.1523/ENEURO.0271-21.2021.
4. Caillaud MC. Anionic Lipids: A Pipeline Connecting Key Players of Plant Cell Division. Front Plant Sci. 2019;10:419. Doi 10.3389/fpls.2019.00419.
5. Coelho M, Oliveira T, Fernandes R. Biochemistry of adipose tissue: an endocrine organ. Arch Med Sci. 2013;9:191–200. Doi 10.5114/aoms.2013.33181.
6. Conde-Green A, Marano AA, Lee ES, Reisler T, Price LA, Milner SM, Granick MS. Fat Grafting and Adipose-Derived Regenerative Cells in Burn Wound Healing and Scarring: A Systematic Review of the Literature. Plast Reconstr Surg. 2016;137:302–12. Doi 10.1097/PRS.0000000000001918.

7. Cui X, Wang Y, Tang Y, Liu Y, Zhao L, Deng J, Xu G, Peng X, Ju S, Liu G al. Seipin ablation in mice results in severe generalized lipodystrophy. Hum Mol Genet. 2011;20:3022–30. Doi 10.1093/hmg/ddr205.
8. Demers G, Roy J, Machuca-Parra AI, Dashtehei Pour Z, Bairamian D, Daneault C, Rosiers CD, Ferreira G, Alquier T, Fulton Set al. Fish oil supplementation alleviates metabolic and anxiodepressive effects of diet-induced obesity and associated changes in brain lipid composition in mice. Int J Obes (Lond). 2020;44:1936–45. Doi 10.1038/s41366-020-0623-6.
9. Ebihara C, Ebihara K, Aizawa-Abe M, Mashimo T, Tomita T, Zhao M, Gumbilai V, Kusakabe T, Yamamoto Y, Aotani Det al. Seipin is necessary for normal brain development and spermatogenesis in addition to adipogenesis. Hum Mol Genet. 2015;24:4238–49. Doi 10.1093/hmg/ddv156.
10. Egea PF. Mechanisms of Non-Vesicular Exchange of Lipids at Membrane Contact Sites: Of Shuttles, Tunnels and, Funnels. Front Cell Dev Biol. 2021;9:784367. Doi 10.3389/fcell.2021.784367.
11. Fullard ME, Morley JF, Duda JE. Olfactory Dysfunction as an Early Biomarker in Parkinson's Disease. Neurosci Bull. 2017;33:515–25. Doi 10.1007/s12264-017-0170-x.
12. Guo J, Yu C, Li H, Liu F, Feng R, Wang H, Meng Y, Li Z, Ju G, Wang J. Impaired neural stem/progenitor cell proliferation in streptozotocin-induced and spontaneous diabetic mice. Neurosci Res. 2010;68:329–36. Doi 10.1016/j.neures.2010.08.012.
13. Hoppela E, Gronroos TJ, Saarikko AM, Tervala TV, Kauhanen S, Nuutila P, Kivinen K, Hartiala P. Fat Grafting Can Induce Browning of White Adipose Tissue. Plast Reconstr Surg Glob Open. 2018;6:e1804. Doi 10.1097/GOX.0000000000001804.
14. Hsieh J. Orchestrating transcriptional control of adult neurogenesis. Genes Dev. 2012;26:1010–21. Doi 10.1101/gad.187336.112.
15. Hu CL, Zeng XM, Zhou MH, Shi YT, Cao H, Mei YA. Kv 1.1 is associated with neuronal apoptosis and modulated by protein kinase C in the rat cerebellar granule cell. J Neurochem. 2008;106:1125–37. Doi 10.1111/j.1471-4159.2008.05449.x.
16. Hunter M, Demarais NJ, Faull RLM, Grey AC, Curtis MA. Layer-specific lipid signatures in the human subventricular zone demonstrated by imaging mass spectrometry. Sci Rep. 2018;8:2551. Doi 10.1038/s41598-018-20793-4.
17. Jing YH, Qi CC, Yuan L, Liu XW, Gao LP, Yin J. Adult neural stem cell dysfunction in the subventricular zone of the lateral ventricle leads to diabetic olfactory defects. Neural Regen Res. 2017;12:1111–8. Doi 10.4103/1673-5374.211190.
18. Kumar JS, Menon VP. Effect of diabetes on levels of lipid peroxides and glycolipids in rat brain. Metabolism. 1993;42:1435–9. Doi 10.1016/0026–0495(93)90195-t.
19. Li G, Zhou L, Zhu Y, Wang C, Sha S, Xian X, Ji Y, Liu G, Chen L. Seipin knockout in mice impairs stem cell proliferation and progenitor cell differentiation in the adult hippocampal dentate gyrus via reduced levels of PPARgamma. Dis Model Mech. 2015;8:1615–24. Doi 10.1242/dmm.021550.
20. Li Y, Yang X, Peng L, Xia Q, Zhang Y, Huang W, Liu T, Jia D. (2022) Role of Seipin in Human Diseases and Experimental Animal Models. Biomolecules 12: Doi 10.3390/biom12060840.

21. Liu L, Jiang Q, Wang X, Zhang Y, Lin RC, Lam SM, Shui G, Zhou L, Li P, Wang Y al. Adipose-specific knockout of SEIPIN/BSCL2 results in progressive lipodystrophy. Diabetes. 2014;63:2320–31. Doi 10.2337/db13-0729.
22. Liu XJ, Wu XY, Wang H, Wang SX, Kong W, Zhang L, Liu G, Huang W. Renal injury in Seipin-deficient lipodystrophic mice and its reversal by adipose tissue transplantation or leptin administration alone: adipose tissue-kidney crosstalk. FASEB J. 2018;32:5550–62. Doi 10.1096/fj.201701427R.
23. Mastrodonato A, Barbati SA, Leone L, Colussi C, Gironi K, Rinaudo M, Piacentini R, Denny CA, Grassi C. Olfactory memory is enhanced in mice exposed to extremely low-frequency electromagnetic fields via Wnt/beta-catenin dependent modulation of subventricular zone neurogenesis. Sci Rep. 2018;8:262. Doi 10.1038/s41598-017-18676-1.
24. McIlroy GD, Suchacki K, Roelofs AJ, Yang W, Fu Y, Bai B, Wallace RJ, De Bari C, Cawthorn WP, Han W al. Adipose specific disruption of seipin causes early-onset generalised lipodystrophy and altered fuel utilisation without severe metabolic disease. Mol Metab. 2018;10:55–65. Doi 10.1016/j.molmet.2018.01.019.
25. Murphy C. Olfactory and other sensory impairments in Alzheimer disease. Nat Rev Neurol. 2019;15:11–24. Doi 10.1038/s41582-018-0097-5.
26. Nakano T, Seino K, Wakabayashi I, Stafforini DM, Topham MK, Goto K. Deletion of diacylglycerol kinase epsilon confers susceptibility to obesity via reduced lipolytic activity in murine adipocytes. FASEB J. 2018;32:4121–31. Doi 10.1096/fj.201701050R.
27. Niu X, Zhao Y, Yang N, Zhao X, Zhang W, Bai X, Li A, Yang W, Lu L. Proteasome activation by insulin-like growth factor-1/nuclear factor erythroid 2-related factor 2 signaling promotes exercise-induced neurogenesis. Stem Cells. 2020;38:246–60. Doi 10.1002/stem.3102.
28. Ogrodnik M, Zhu Y, Langhi LGP, Tchkonia T, Kruger P, Fielder E, Victorelli S, Ruswhandi RA, Giorgadze N. Pirtskhalava Tet al (2019) Obesity-Induced Cellular Senescence Drives Anxiety and Impairs Neurogenesis. Cell Metab 29: 1061–1077 e1068 Doi 10.1016/j.cmet.2018.12.008.
29. Ottone C, Parrinello S. Multifaceted control of adult SVZ neurogenesis by the vascular niche. Cell Cycle. 2015;14:2222–5. Doi 10.1080/15384101.2015.1049785.
30. Payne VA, Grimsey N, Tuthill A, Virtue S, Gray SL, Dalla Nora E, Semple RK, O'Rahilly S, Rochford JJ. The human lipodystrophy gene BSCL2/seipin may be essential for normal adipocyte differentiation. Diabetes. 2008;57:2055–60. Doi 10.2337/db08-0184.
31. Qian Y, Yin J, Hong J, Li G, Zhang B, Liu G, Wan Q, Chen L. Neuronal seipin knockout facilitates Abeta-induced neuroinflammation and neurotoxicity via reduction of PPARgamma in hippocampus of mouse. J Neuroinflammation. 2016;13:145. Doi 10.1186/s12974-016-0598-3.
32. Schneiter R, Choudhary V. Seipin collaborates with the ER membrane to control the sites of lipid droplet formation. Curr Opin Cell Biol. 2022;75:102070. Doi 10.1016/j.ceb.2022.02.004.
33. Shin J, Berg DA, Zhu Y, Shin JY, Song J, Bonaguidi MA, Enikolopov G, Nauen DW, Christian KM. Ming GLet al (2015) Single-Cell RNA-Seq with Waterfall Reveals Molecular Cascades underlying Adult Neurogenesis. Cell Stem Cell 17: 360–372 Doi 10.1016/j.stem.2015.07.013.

34. Sighinolfi G, Clark S, Blanc L, Cota D, Rhourri-Frih B. Mass spectrometry imaging of mice brain lipid profile changes over time under high fat diet. Sci Rep. 2021;11:19664. Doi 10.1038/s41598-021-97201-x.
35. Staps P, Rizzo WB, Vaz FM, Bugiani M, Giera M, Heijs B, van Kampen AHC, Pras-Raves ML, Breur M, Groen Aet al. Disturbed brain ether lipid metabolism and histology in Sjogren-Larsson syndrome. J Inherit Metab Dis. 2020;43:1265–78. Doi 10.1002/jimd.12275.
36. Steinhart R, Kazimirsky G, Okhrimenko H, Ben-Hur T, Brodie C. PKCepsilon induces astrocytic differentiation of multipotential neural precursor cells. Glia. 2007;55:224–32. Doi 10.1002/glia.20454.
37. Tagawa K, Homma H, Saito A, Fujita K, Chen X, Imoto S, Oka T, Ito H, Motoki K, Yoshida Cet al. Comprehensive phosphoproteome analysis unravels the core signaling network that initiates the earliest synapse pathology in preclinical Alzheimer's disease brain. Hum Mol Genet. 2015;24:540–58. Doi 10.1093/hmg/ddu475.
38. Tian Y, Bi J, Shui G, Liu Z, Xiang Y, Liu Y, Wenk MR, Yang H, Huang X. Tissue-autonomous function of Drosophila seipin in preventing ectopic lipid droplet formation. PLoS Genet. 2011;7:e1001364. Doi 10.1371/journal.pgen.1001364.
39. Walker IM, Fullard ME, Morley JF, Duda JE. Olfaction as an early marker of Parkinson's disease and Alzheimer's disease. Handb Clin Neurol. 2021;182:317–29. Doi 10.1016/B978-0-12-819973-2.00030 – 7.
40. Wang H, Kazanietz MG. p23/Tmp21 differentially targets the Rac-GAP beta2-chimaerin and protein kinase C via their C1 domains. Mol Biol Cell. 2010;21:1398–408. Doi 10.1091/mbc.E09-08-0735.
41. Wang H, Xu PF, Li JY, Liu XJ, Wu XY, Xu F, Xie BC, Huang XM, Zhou ZH. Kayoumu Aet al (2019) Adipose tissue transplantation ameliorates lipodystrophy-associated metabolic disorders in seipin-deficient mice. Am J Physiol Endocrinol Metab 316: E54-E62 Doi 10.1152/ajpendo.00180.2018.
42. Willette AA, Bendlin BB, Starks EJ, Birdsill AC, Johnson SC, Christian BT, Okonkwo OC, La Rue A, Hermann BP. Koscik RLet al (2015) Association of Insulin Resistance With Cerebral Glucose Uptake in Late Middle-Aged Adults at Risk for Alzheimer Disease. JAMA Neurol 72: 1013–1020 Doi 10.1001/jamaneurol.2015.0613.
43. Wood PL, Medicherla S, Sheikh N, Terry B, Phillipps A, Kaye JA, Quinn JF, Woltjer RL. Targeted Lipidomics of Fontal Cortex and Plasma Diacylglycerols (DAG) in Mild Cognitive Impairment and Alzheimer's Disease: Validation of DAG Accumulation Early in the Pathophysiology of Alzheimer's Disease. J Alzheimers Dis. 2015;48:537–46. Doi 10.3233/JAD-150336.
44. Zhang Z, Zhang B, Wang X, Zhang X, Yang QX, Qing Z, Lu J, Bi Y, Zhu D. Altered Odor-Induced Brain Activity as an Early Manifestation of Cognitive Decline in Patients With Type 2 Diabetes. Diabetes. 2018;67:994–1006. Doi 10.2337/db17-1274.
45. Zhao H, Li Y, Wang J, Cheng M, Zhao Z, Zhang H, Wang C, Wang J, Qiao Y, Wang J. Dual-Ion-Mode MALDI MS Detection of Small Molecules with the O-P,N-Doped Carbon/Graphene Matrix. ACS Appl Mater Interfaces. 2018;10:37732–42. Doi 10.1021/acsami.8b14643.

46. Zhao Y, Liu X, He Z, Niu X, Shi W, Ding JM, Zhang L, Yuan T, Li A, Yang W al. Essential role of proteasomes in maintaining self-renewal in neural progenitor cells. Sci Rep. 2016;6:19752. Doi 10.1038/srep19752.
47. Zhou L, Chen T, Li G, Wu C, Wang C, Li L, Sha S, Chen L, Liu G, Chen L. Activation of PPARgamma Ameliorates Spatial Cognitive Deficits through Restoring Expression of AMPA Receptors in Seipin Knock-Out Mice. J Neurosci. 2016;36:1242–53. Doi 10.1523/JNEUROSCI.3280-15.2016.
48. Zhou L, Yin J, Wang C, Liao J, Liu G, Chen L. Lack of seipin in neurons results in anxiety- and depression-like behaviors via down regulation of PPARgamma. Hum Mol Genet. 2014;23:4094–102. Doi 10.1093/hmg/ddu126.
49. Zhu L, Wang P, Sun YJ, Xu MY, Wu YJ. Disturbed phospholipid homeostasis in endoplasmic reticulum initiates tri-o-cresyl phosphate-induced delayed neurotoxicity. Sci Rep. 2016;6:37574. Doi 10.1038/srep37574.

Tables

Table 1 Antibodies used in this study

Antibodies	Species	Application	Dilution	Company & Catalog number
Rabbit anti-DCX	Rabbit	IF	1:200	Cell Signaling technology, Cat# 4604
Rabbit anti-Ki67	Rabbit	IF	1:400	Abcam, Cat# ab15580
Rabbit anti-NeuN	Rabbit	IF	1:400	Proteintech Group, Cat# 26975-1-AP
Mouse anti-BrdU	Mouse	IF	1:200	Abclonal, Cat# A1482
Mouse anti-Tuj1	Mouse	IF	1:300	Sigma-Aldrich, Cat# MAB1637
Goat anti-rabbit IgG H & L (Alexa Fluor 555)	Rabbit	IF	1:200	Invitrogen, Cat# A-21429
Goat anti-mouse IgG H & L (Alexa Fluor 488)	Mouse	IF	1:200	Invitrogen, Cat# A-28175
Goat anti-mouse IgG H & L (Alexa Fluor 555)	Mouse	IF	1:200	Invitrogen, Cat# A-21424
Mouse anti-PKCα	Mouse	WB	1:1000	Sigma-Aldrich, Cat# sc-8393
Mouse anti-β-actin	Mouse	WB	1:4000	Sangon Biotech, Cat# A1978
Rabbit IgG, HRP	Rabbit	WB	1:5000	ZSGB-BIO, Cat# ZB-2306
Mouse IgG, HRP	Mouse	WB	1:5000	ZSGB-BIO, Cat# ZB-2305

Figures

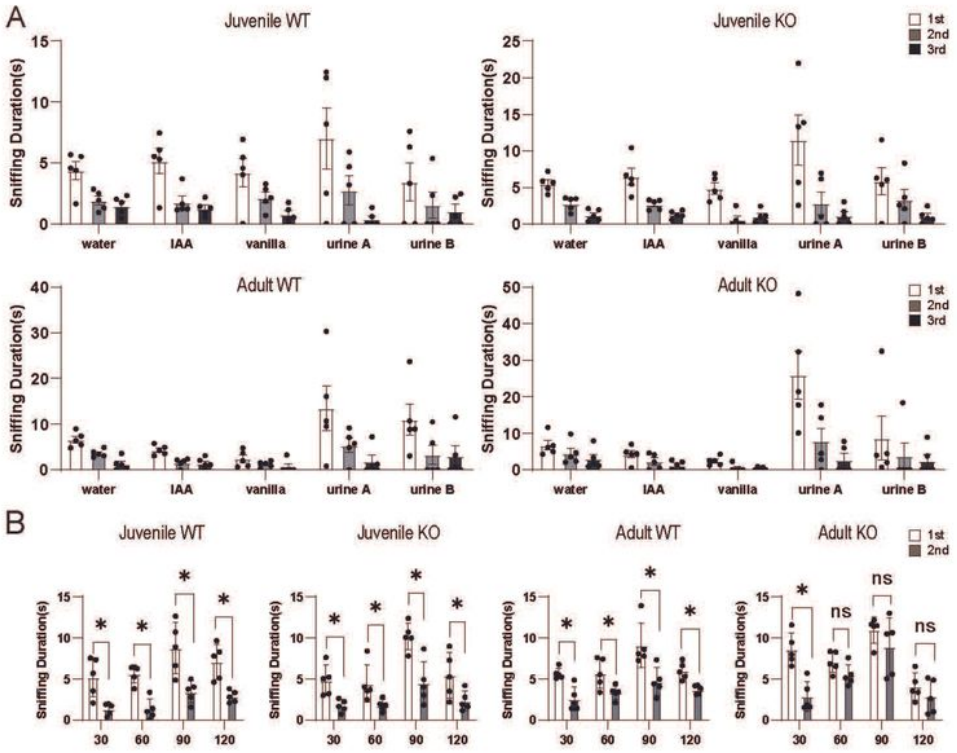

Figure 1

Olfactory function assay of KO and WT mice.

A: Time spent investigating mineral oil, IAA, vanilla, female mice urine and male mice urine (n = 5). **B**: The sniffing duration for mice presented with the same odorants twice at the indicated time intervals (n = 5). Data were shown as means ± SD. *$p < 0.05$.

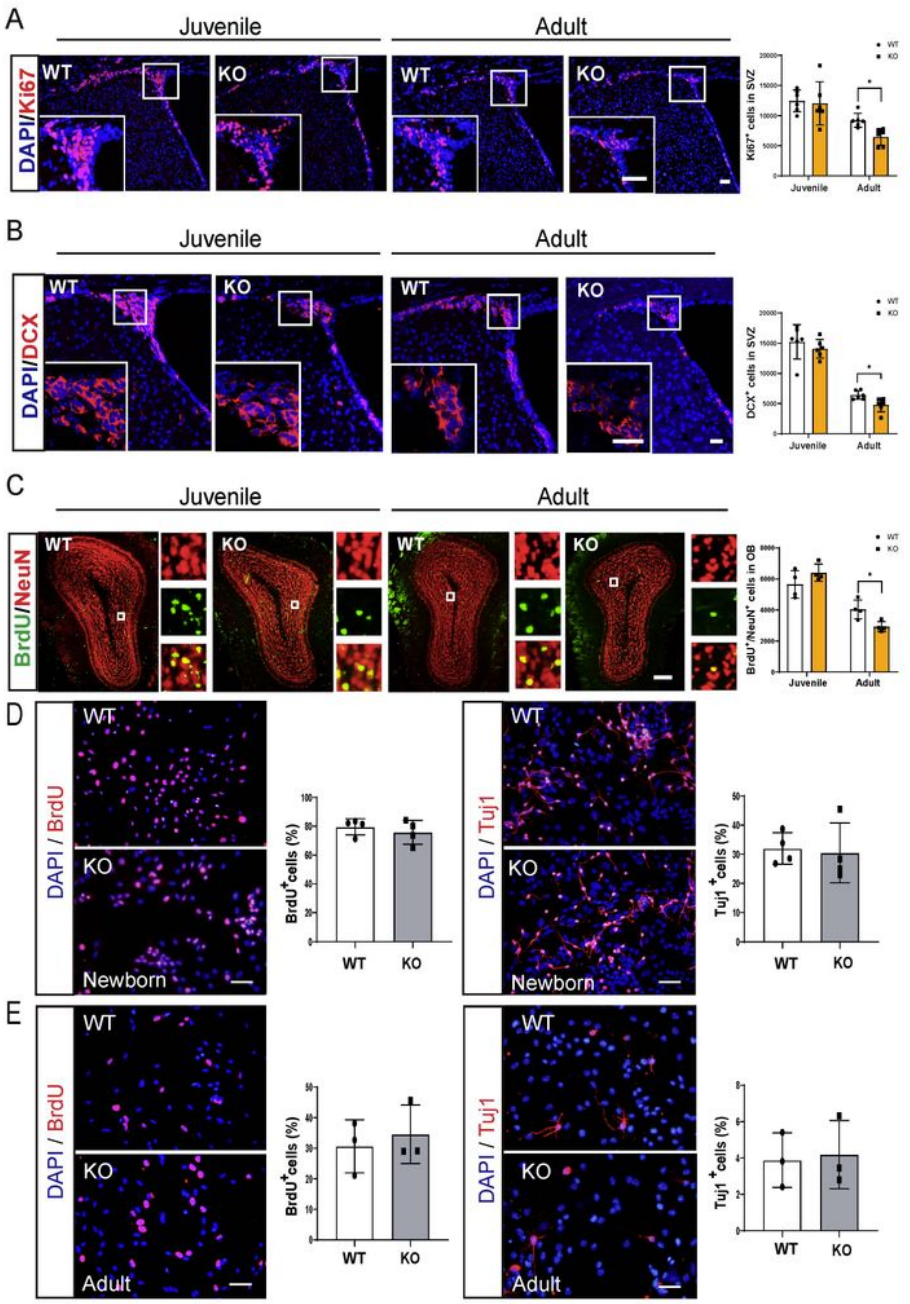

Figure 2

SVZ neurogenesis in adult KO mice.

A - C: Immunofluorescence analysis for Ki67, DCX, and BrdU/NeuN in SVZ (A and B) and olfactory bulb (C) of juvenile and adult WT and KO mice, respectively. The right panel corresponded to a higher magnification view of the boxed region shown in the merged image. n = 6 (A and B), Scale bar = 50 μm in (A), Scale bar = 25 μm in (B); n = 4, Scale bar = 200 μm in (C). **D and E**: The proliferation and differentiation capacity of cells as determined by BrdU staining and Tuj1 staining in NSCs from neonatal (D) and adult mice (E), respectively. DAPI was used as a nuclear counterstain. Scale bar=50 μm in (D and E). Data was shown as means ± SD. *$p < 0.05$ vs. adult WT.

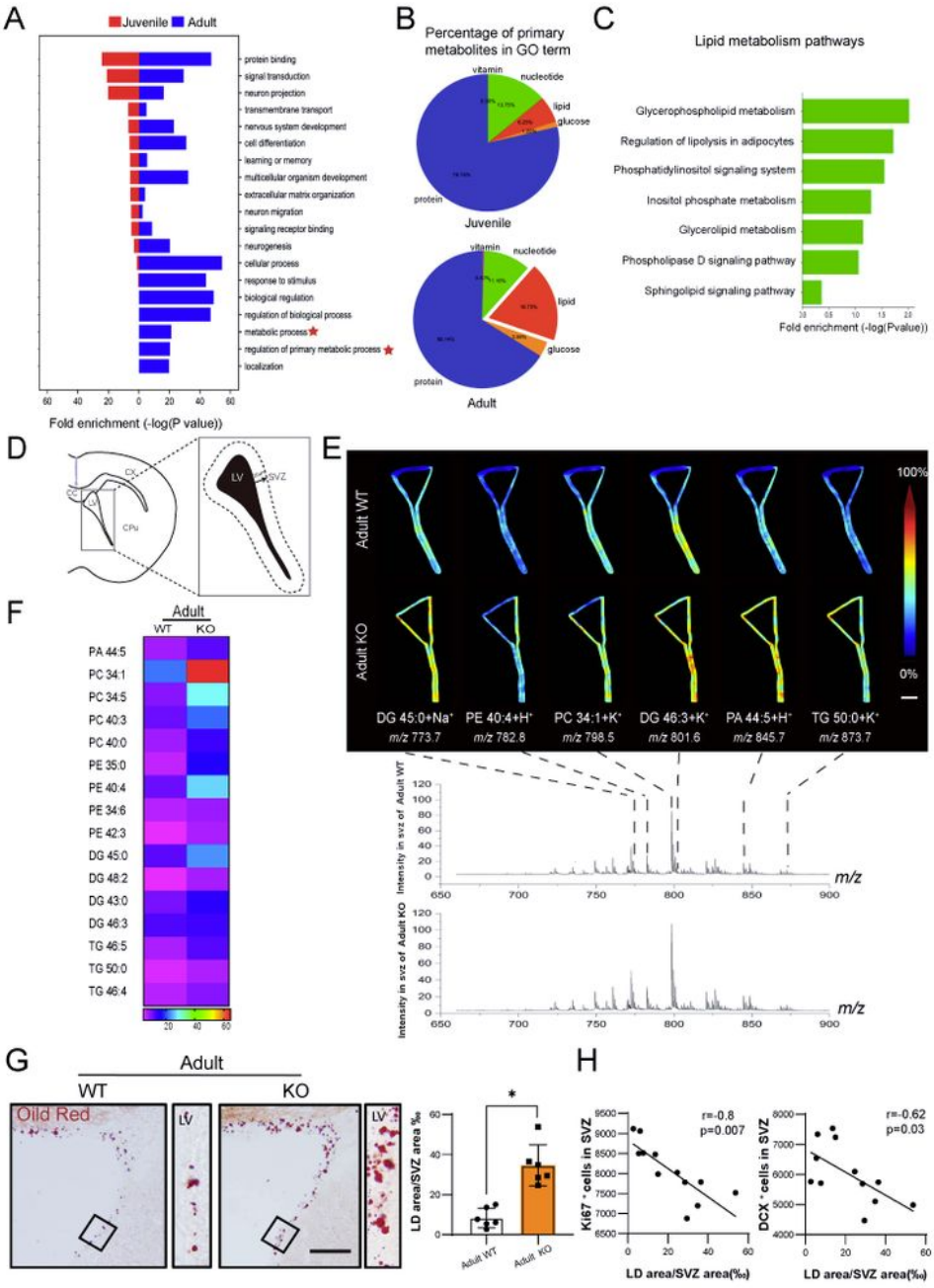

Figure 3

Altered lipid metabolism in the SVZ of adult mice.

A: GO analysis of genes in SVZ of KO and WT mice. **B**: Pie charts to show the percentage of lipid metabolism in SVZ primary metabolism of adult and juvenile KO mice. **C**: KEGG pathway analysis showing the lipid metabolism-related DEGs, including glycerophospholipid, phospholipase D, and

sphingolipid signaling pathways between adult KO and WT mice. **D**: Pattern diagram of SVZ region by MALDI-TOF MS analysis. CX: cortex, CPu: caudate putamen, CC: corpus callosum, LV: lateral ventricle, SVZ: subventricular zone. **E**: MALDI-TOF MS showing significantly accumulated lipids in the SVZ of adult KO mice and their representative m/z ratio peaks. Scale bar = 100 μm. **F**: Heatmap analysis showing the most significantly accumulated lipid component in the SVZ of adult KO mice (n = 3). PA: phosphatidic acid, PC: phosphatidylcholine, PE phosphatidylethanolamine, DG: diacylglycerol, TG: triglyceride. **G**: Oil Red O detection of LD in the SVZ of the adult brain of KO mice (n = 6), Scale bar = 50 μm. **H**: Pearson correlations analyses between neurogenesis impairment and the area of LD accumulation (n = 6). Data were shown as means ± SD. *$p < 0.05$ vs. adult WT.

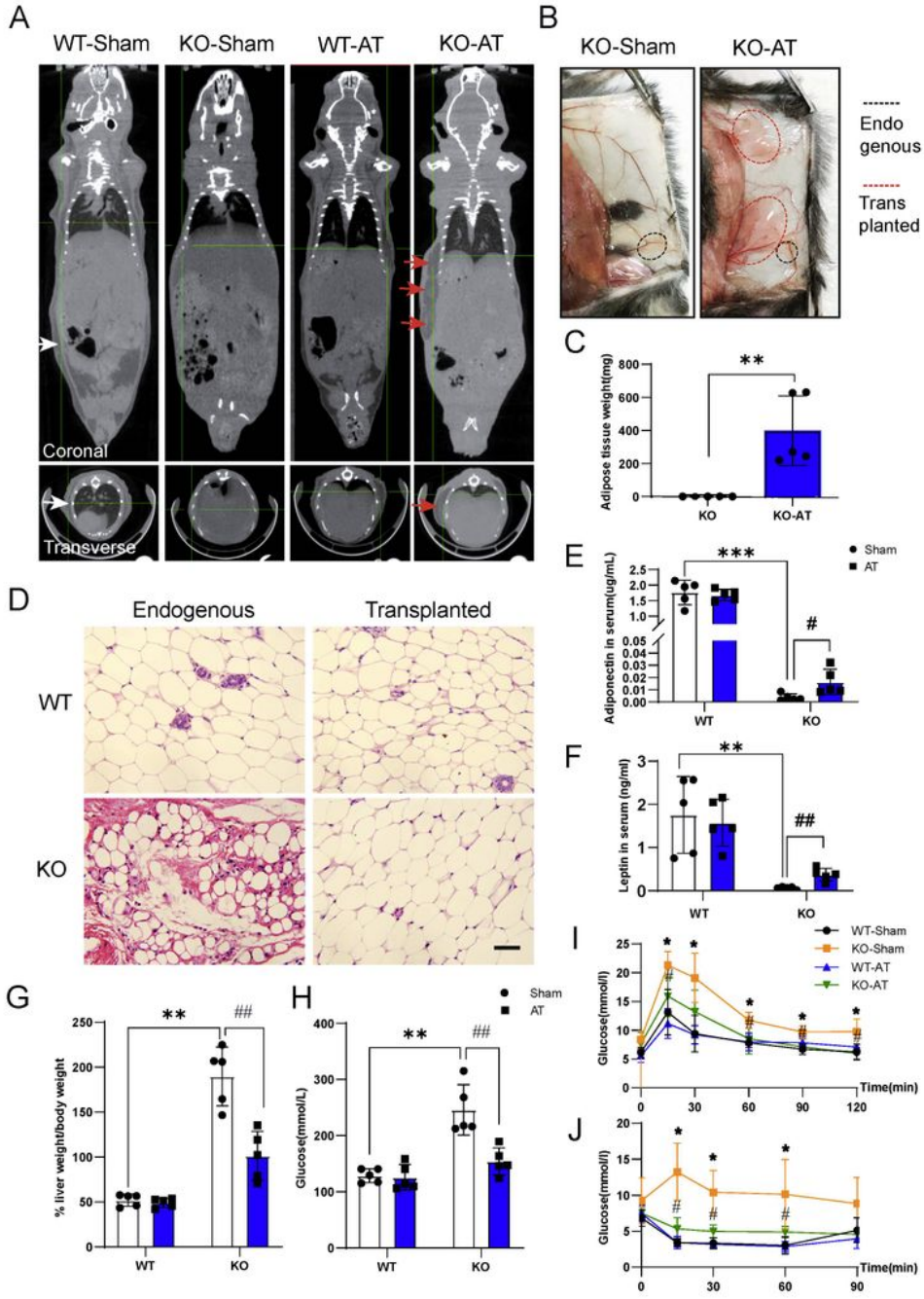

Figure 4

AT impact on systemic metabolic homeostasis in KO mice.

A: Representative CT scan images from coronal and transverse views from each group. **B**: Representative gross appearance of subcutaneous adipose tissue. **C**: CT scan showing the weight of surviving adipose tissue four months after AT (n = 5). $^{**}p < 0.01$ vs. KO-sham. **D**: Adipose tissue sections stained with HE to

show the morphology of transplanted adipose tissues. Scale bar = 50 μm. **E and F**: The serum adiponectin and leptin levels in the KO mice after AT (n = 5). ** $p < 0.01$ vs. WT-Sham, *** $p < 0.001$ vs. WT-Sham, # $p < 0.05$ vs. KO-Sham, ## $p < 0.01$ vs. KO-Sham. **G and H**: The ratio of liver weight to body weight and fasting blood glucose levels in the KO mice after AT (n = 5). ** $p < 0.01$ vs. WT-Sham, ## $p < 0.01$ vs. KO-Sham. **I and J**: Blood glucose levels after AT in KO mice with glucose load (I) and insulin injection (J). n = 5, * $p < 0.05$ vs. WT-Sham, # $p < 0.05$ vs. KO-Sham. Data were shown as means ± SD.

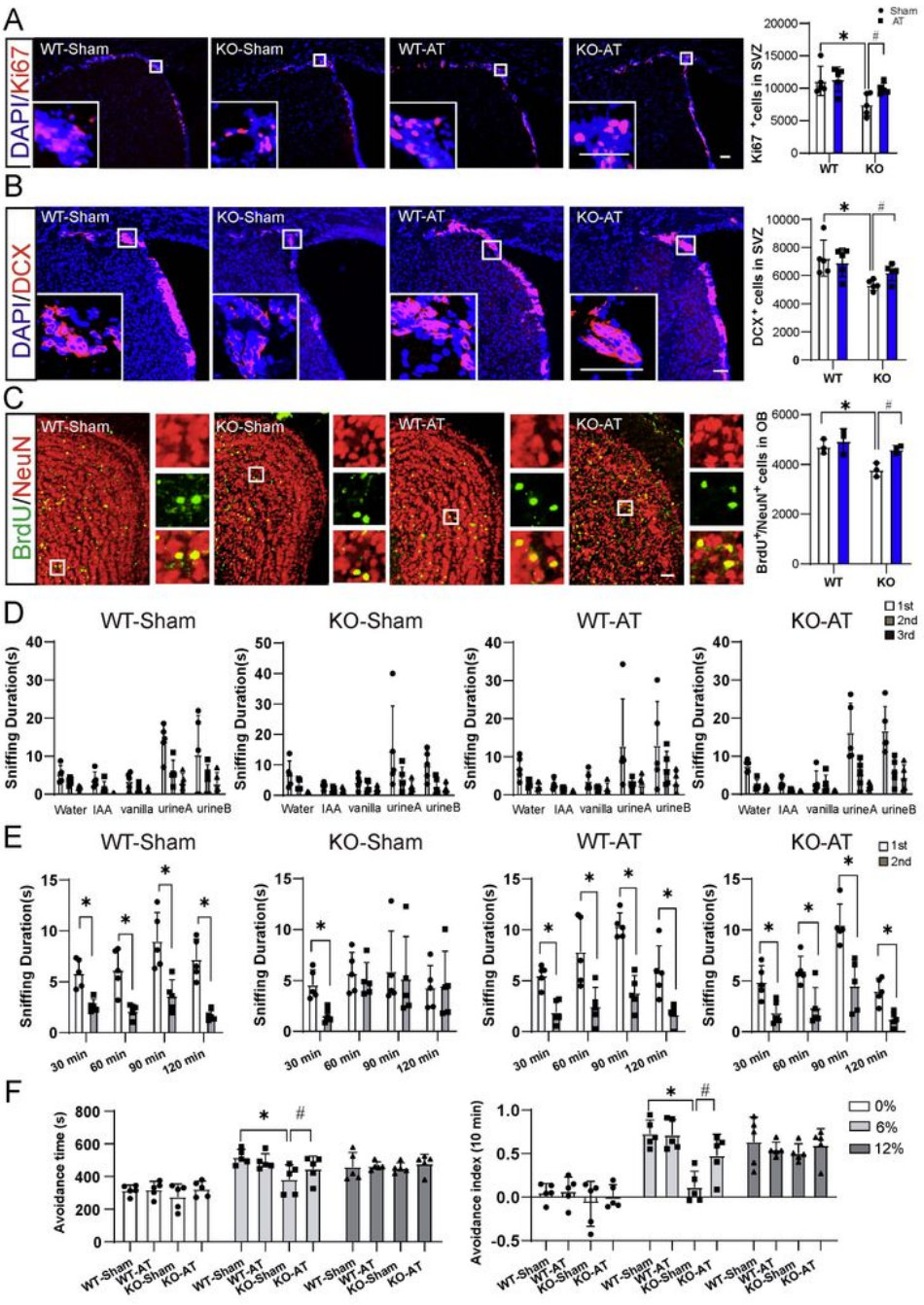

Figure 5

SVZ neurogenesis and neurological function in adult KO mice after AT.

A-C: Immunofluorescence staining and analysis of Ki67 (A), DCX (B) and $BrdU^+/NeuN^+$ (C) in the SVZ and olfactory bulb granular layer of each group to show neurogenesis of adult KO mice. n = 5, Scale bar = 50 μm in (A and B); n = 3, Scale bar = 50 μm in (C). *$p < 0.05$ vs. WT-sham, #$p < 0.05$ vs. KO-sham. **D**:

Olfactory habituation/dishabituation assay of KO and WT mice with or without AT (n = 5). **E**: Short-term olfactory memory test KO mice before with or without AT (n = 5). *$p < 0.05$ vs.1st. **F**: Odor avoidance tests in the presence of different doses of nTMT in KO mice before with or without AT (n = 5). *$p < 0.05$ vs. WT-sham, #$p < 0.05$vs. KO-sham. Data were shown as means ± SD.

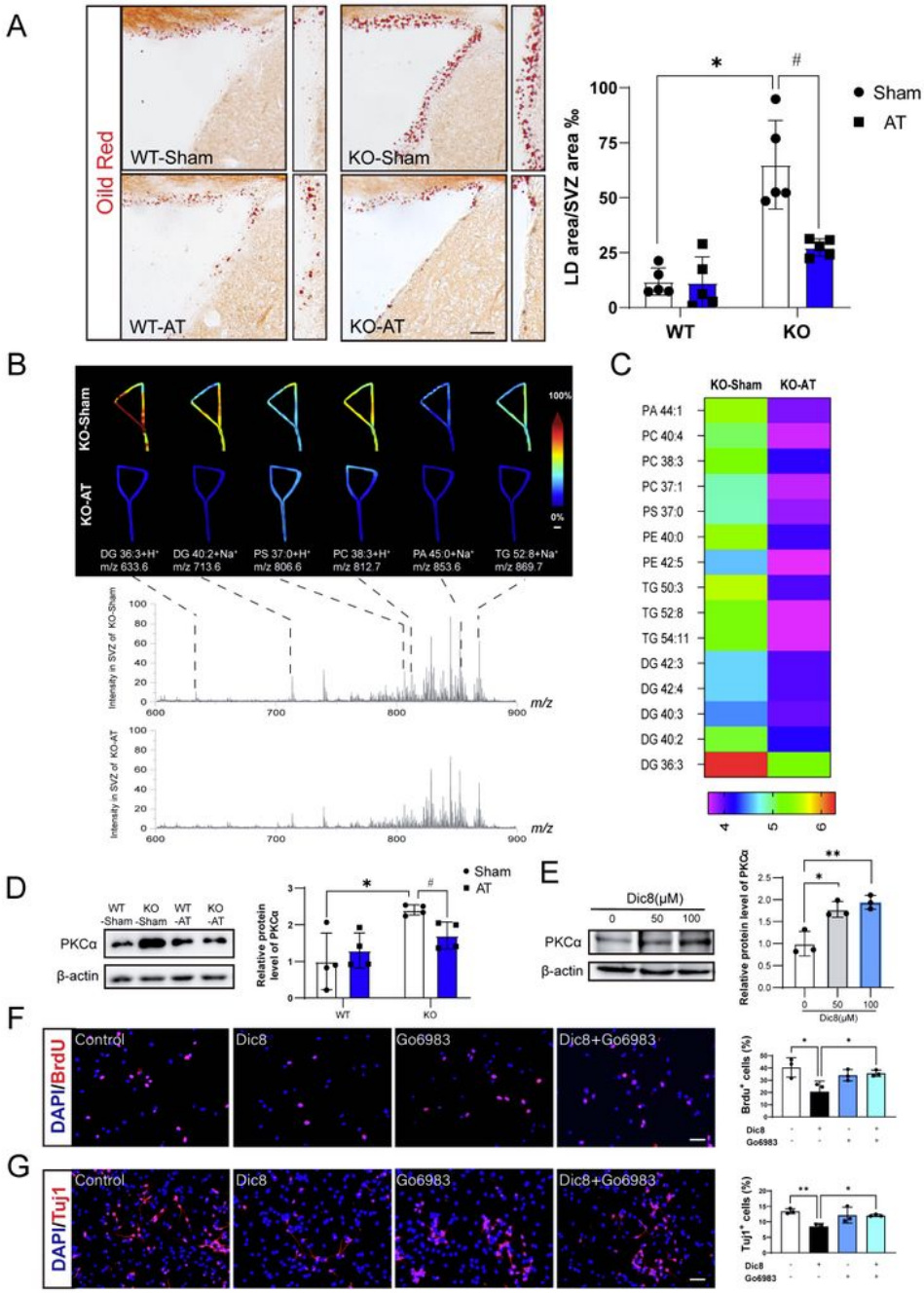

Figure 6

AT impacting the lipid metabolism of and activity of neurogenesis of NSCs via the DG-PKCα pathway.

A: Oil Red staining shows LD in SVZ of KO and WT mice with or without AT (n = 5). *$p < 0.05$ vs. WT-sham, #$p < 0.05$ vs. KO-sham. Scale bar=50 μm. **B and C**: Imaging mass spectrometry (B) and heatmap (C) analysis of lipid profiles in SVZ of KO mice with or without AT to show significantly reduced lipids (n = 3). Scale bar=100 μm (B); PA: phosphatidic acid, PC: phosphatidylcholine, PE phosphatidylethanolamine, DG: diacylglycerol, TG: triglyceride (C). **D and E**: Western blotting to show the protein expression of PKCα in SVZ of KO mice before and after AT (D) and in NSCs derived from SVZ treated with 0, 50, 100 μM DiC8 (E). *$p < 0.05$ vs. WT-sham, #$p < 0.05$ vs. KO-sham. **F and G**: Immunofluorescence analysis for BrdU (F) and Tuj1 (G) to show the impact of DiC8 (100 μM) and PKCα inhibitor on proliferation and differentiation of NSCs derived from SVZ. Scale bar=50 μm. *$p < 0.05$. Data were shown as means ± SD.

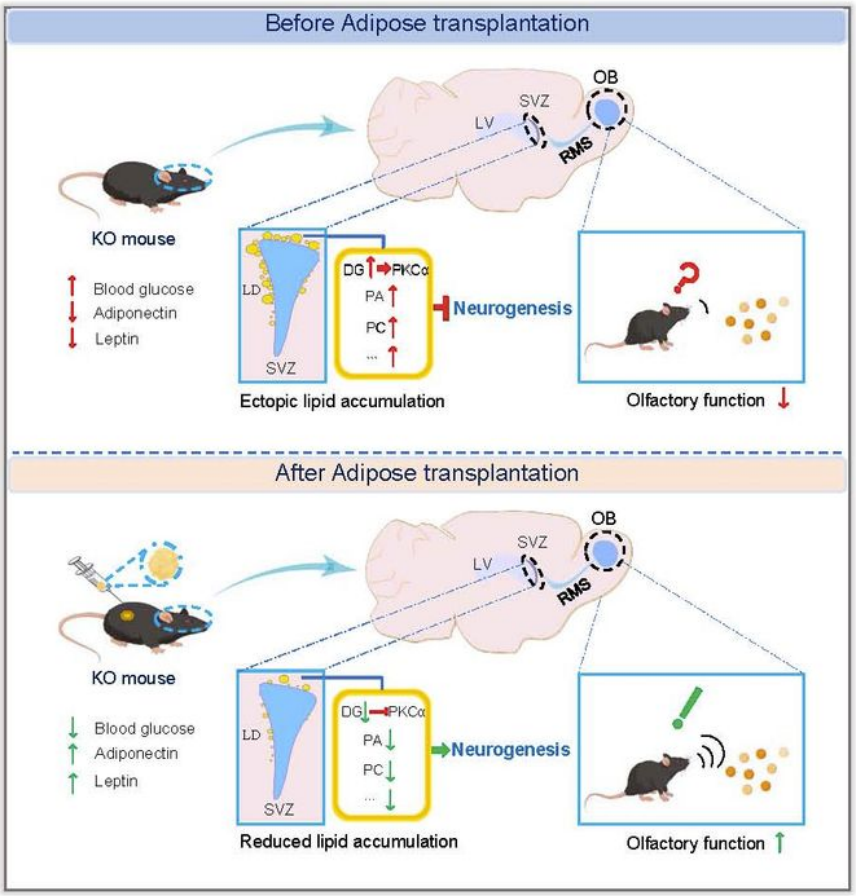

Figure 7

Schematic figure to show the phenotypes of Seipin deficiency on neurogenesis and olfactory function and the rescue effect of adipose transplantation.

Seipin deficiency led to lipid metabolites accumulation in SVZ, which compromised neurogenesis and olfactory function. AT rescued the above phenotypes. OB: olfactory bulb, SVZ: subventricular zone, LV:

lateral ventricle, RMS: rostral migratory stream, AT: adipose tissue transplantation, LD: lipid droplets, DG: diacylglycerol, PA: phosphatidic acid, PC: phosphatidylcholine.

Supplementary Files

This is a list of supplementary files associated with this preprint. Click to download.

- SupplementaryFigures.docx
- fig.S1.jpg